Electronic Supplementary Material (ESI) for ChemComm.


**Supporting Information**

# Genetically Encoded RNA-based Sensors for Intracellular Imaging of Silver Ions

Qikun Yu,[‡a] Jing Shi,[‡ab] Aruni P. K. K. Karunanayake Mudiyanselage,[a] Rigumula Wu,[a] Bin Zhao,[†] Ming Zhou,[*b] and Mingxu You[*a]

[a] Department of Chemistry, University of Massachusetts, Amherst, Massachusetts 01003, USA

[b] Sate Key Laboratory of Tribology, Tsinghua University, Beijing, 10084, China

*Corresponding author: mingxuyou@chem.umass.edu;

zhouming@tsinghua.edu.cn

**This file includes:**

**Materials and Methods:**

**Reagents:** All the chemicals were purchased from Sigma or Fisher Scientific unless otherwise noted. The PVP (40kDa)-coated silver nanoparticles were purchased from NanoComposix (San Diego, CA). All the RNA structures were designed using a NUPACK software. DNA oligonucleotides were synthesized and purified by W. M. Keck Oligonucleotide Synthesis Facility (Yale University School of Medicine) and Integrated DNA Technologies (Coralville, IA). Oligonucleotides were dissolved at 100 μM concentration in 10 mM Tris–HCl, 0.1 mM EDTA at pH = 7.5 and stored at -20°C. Double stranded DNA template and non-template strands for *in vitro* transcription were prepared by PCR amplification using an Eppendorf Mastercycler. The PCR product was gel purified and cleaned using a QIAquick PCR purification kit (Qiagen, Germantown, MD). All the concentrations of nucleic acids were measured using a NanoDrop One UV-Vis spectrophotometer. All RNAs for the *in vitro* test were transcribed using a HiScribe™ T7 high yield RNA synthesis kit (New England BioLabs, Ipswich, MA) and then column purified. All the RNA molecules were prepared into aliquots and stored at -20°C for immediate usage or at -80°C for long-term storage.

**Fluorescence assay:** All the in vitro fluorescence measurements were conducted in a PTI fluorimeter (Horiba, New Jersey, NJ). Fluorescence assays were conducted in a Broccoli folding buffer consisting of 40 mM HEPES, 100 mM KCl, 0.1% DMSO and 1 mM $MgCl_2$, at pH=7.5. 1 μM RNA and 20 μM DFHBI-1T was used for these measurements. All the samples have been incubated at room temperature for 2 h before taking the measurements. The 495–520 nm emission spectra were collected by exciting at 480 nm. Kinetic assays were conducted by exciting at 480 nm and collecting fluorescence at 503 nm. All the data were plotted with the Origin software.

**Vector construction:** S1 and Broccoli sequence with T7 promoter and terminator were cloned into a pET28c vector. The vector was first digested with BglII and XhoI restriction enzymes (New England BioLabs). After gel purification, the digested vector was ligated with a similarly digested S1 or Broccoli insert using T4 DNA ligase (New England BioLabs). The ligated product was transform into BL21 (DE3)* cells (New England BioLabs) and screened based on kanamycin resistance. All these plasmids were isolated and confirmed by Sanger sequencing at Genewiz, NJ.

**Cellular imaging and data analysis:** Cellular imaging was performed according to a previously established protocol (R. L. Strack, W. Song and S. R. Jaffrey, *Nat. Protoc.*, 2014, **9**, 146–155.). The S1/Broccoli-expressed BL21 (DE3)* cells were grown in LB media at 37°C until the optical density at 600 nm reaching 0.4–0.5, and then 1 mM IPTG was added for a 2 h induction before the confocal imaging. After induction, the cells were adhered to poly-L-lysine pretreated glass bottom dish at 37°C for 45 min, and then 200 μM DFHBI-1T and 10 μg/mL propidium iodide (PI) were added at room temperature 30 min before imaging. All fluorescence images were collected with a NIS-Elements AR software using a Yokogawa spinning disk confocal on a Nikon Eclipse-TI inverted microscope. Broccoli and S1 RNA sensors were excited with a 488 nm laser line. PI was excited with a 561 nm laser line. 60×

oil immersion objective was used. Data analysis was performed with the NIS-Elements AR Analysis software. Data calculation and fitting was done using the Origin software. The individual cell fluorescence analysis was done using the ImageJ software.

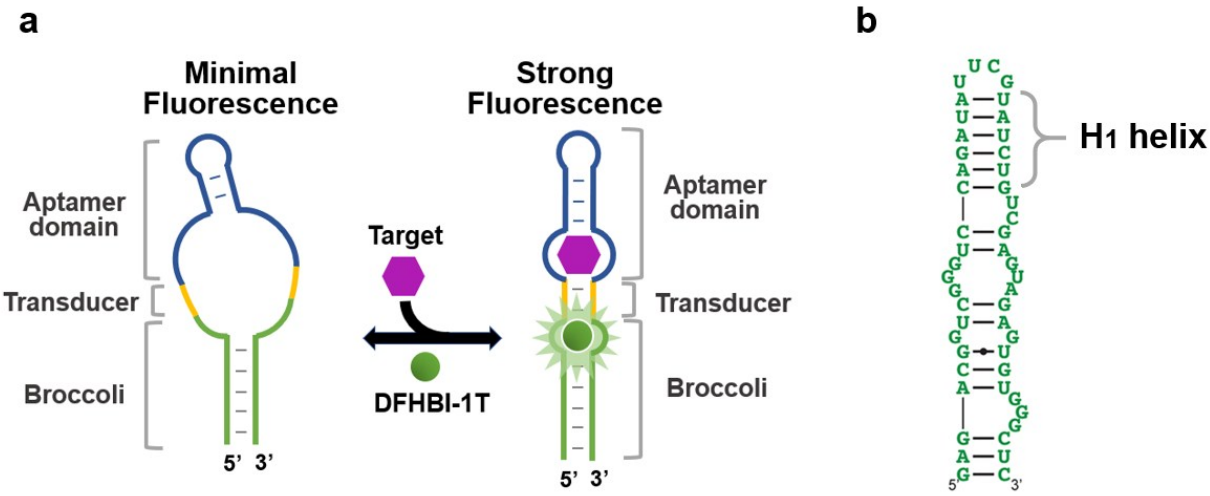


**Figure S1.** (a) Schematic of Broccoli-based allosteric sensor. Typical RNA allosteric sensor comprises Broccoli (green), a transducer (orange), and a target-binding aptamer (blue). The target-binding aptamer is linked through the transducer into a structurally critical stem region ($H_1$ helix) of Broccoli (b). Target binding to the aptamer promotes stabilization of the transducer stem, enables Broccoli to fold and activates DFHBI-1T fluorescence. (b) Sequence and secondary structure of Broccoli aptamer. The $H_1$ helix is a critical stem region on top of DFHBI-1T binding pocket.

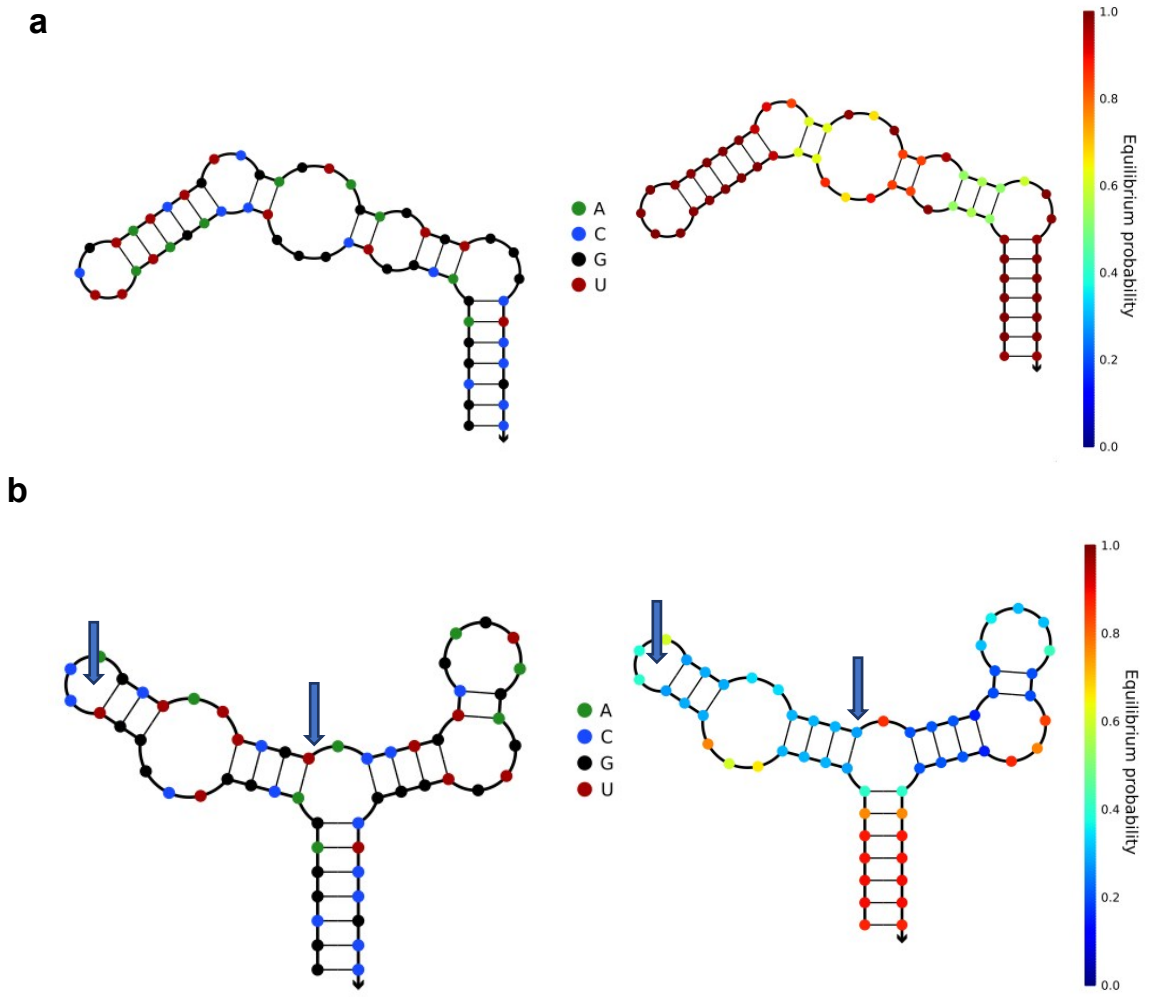


**Figure S2.** NUPACK predicted secondary structure of C-C mismatch-incorporated Broccoli. (a) Predicted secondary structure of Broccoli with color-coded bases (left) and shaded equilibrium probability (right). (b) Predicted secondary structure of S1 with one A-U base pair mutation in the $H_1$ helix of Broccoli to the C-C mismatch (blue arrows). The overall predicted secondary structure was dramatically changed after mutation (left). Based on the low equilibrium probability of forming stable base pairs around the two mutated cytosine bases (right), there is indeed a chance to form C-$Ag^+$-C metallo base pairs.

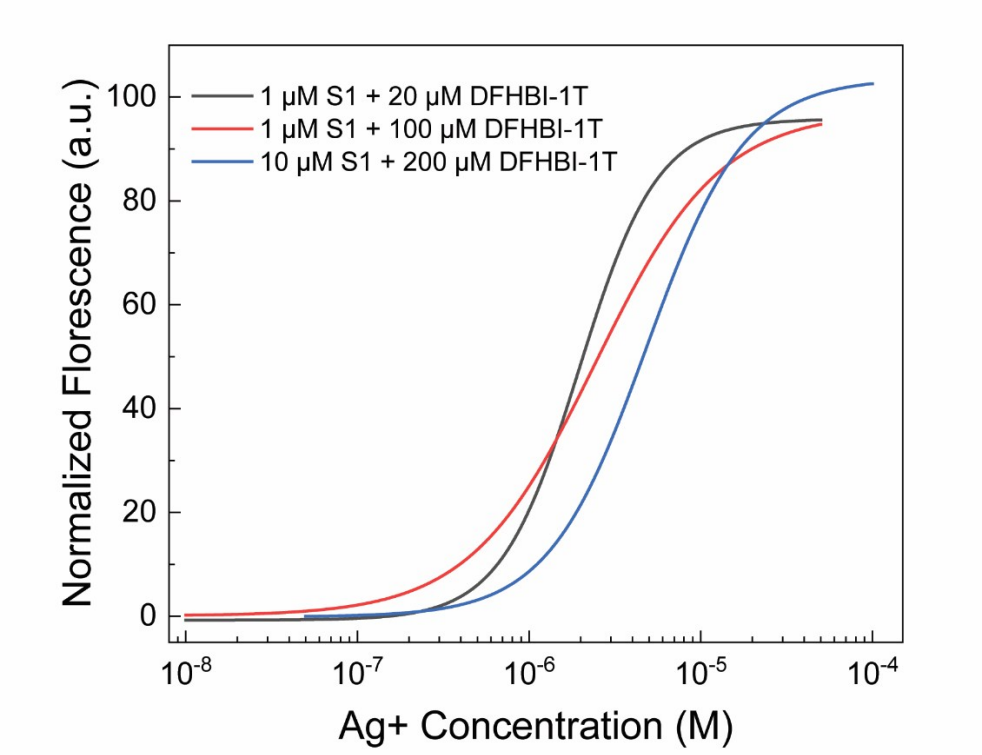


**Figure S3.** Dose response curve of the S1 sensor under different RNA or DFHBI-1T concentration. The dose responsive curves were fitted the same way as Fig. 1c. From the result we can tell that, the detection range will not be influenced obviously by only increasing DFHBI-1T concentration (red line), compared to the normal condition we used (black line). While by increasing the RNA concentration from 1 μM to 10 μM with the same fold of excess DFHBI-1T (blue line), the detection range shifted to larger concentration.

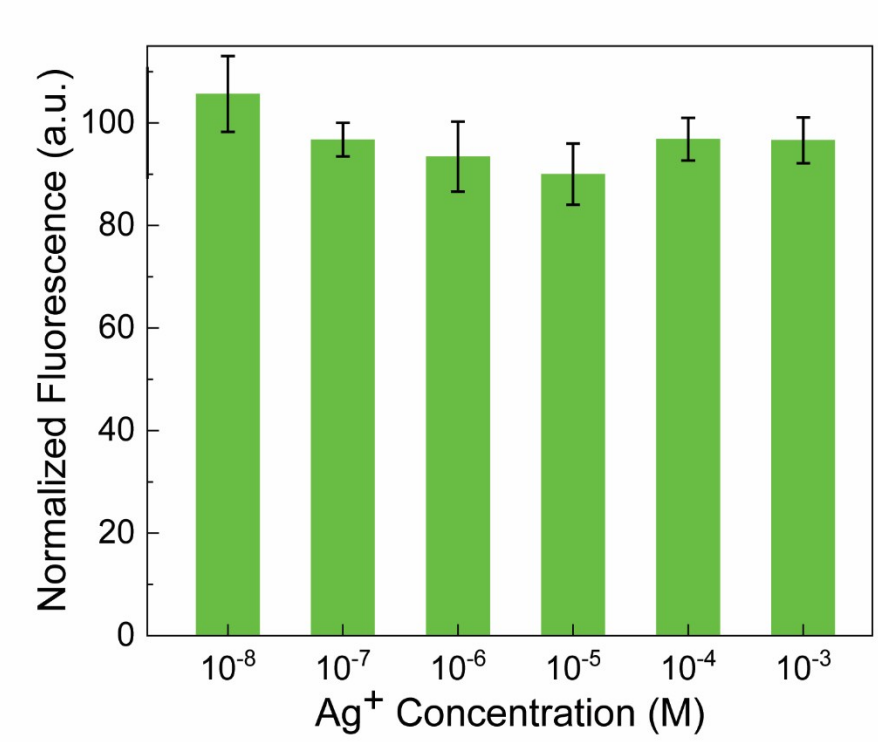


**Figure S4.** Broccoli fluorescence at 2 h after adding various amounts of $AgNO_3$. All spectra were measured in a solution containing 1 μM RNA and 20 μM DFHBI-1T and normalized based on the Broccoli fluorescence without adding $AgNO_3$. The results shown that there is no obvious difference after adding $AgNO_3$ from 10 nM to 1 mM towards Broccoli signal.

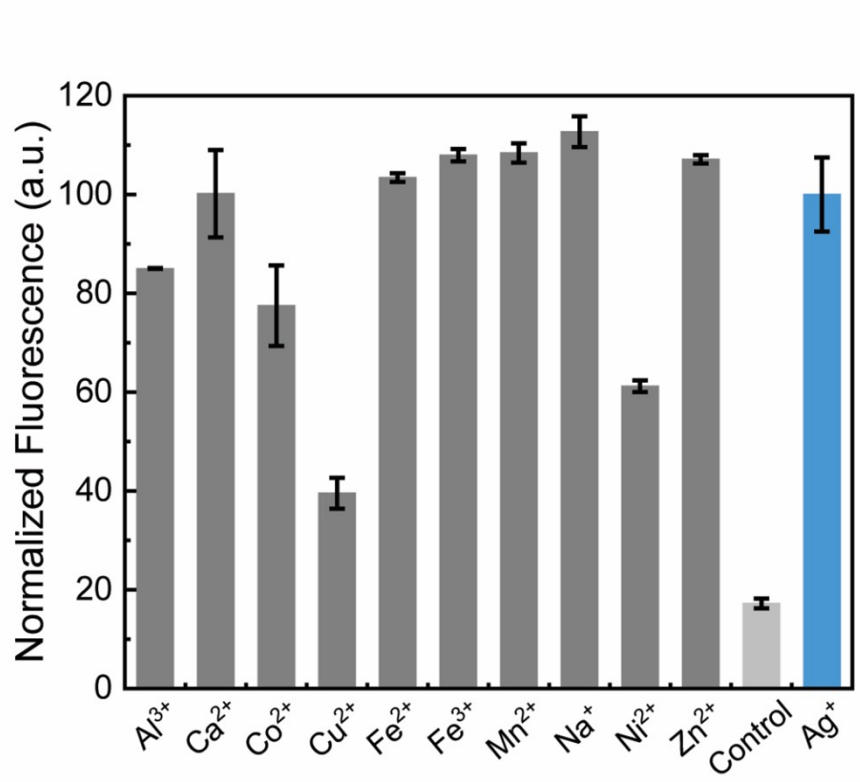


**Figure S5.** Influence of other cations on the fluorescence detection of $Ag^+$. All the ions were tested at 10 μM in a solution containing 10 μM $Ag^+$, 1 μM S1, 20 μM DFHBI-1T, 100 mM $K^+$ and 1 mM $Mg^{2+}$ at pH 7.5. Control was measured in this solution without adding $Ag^+$ or other tested cations. Shown are the mean and S.E.M. values from three independent replicates. All these ions, except $Cu^{2+}$ and $Ni^{2+}$, will not influence the detection of $Ag^+$ at the tested 10 μM level. While we believe that the low physiological concentrations of $Cu^{2+}$ and $Ni^{2+}$ should not influence the S1 signal.

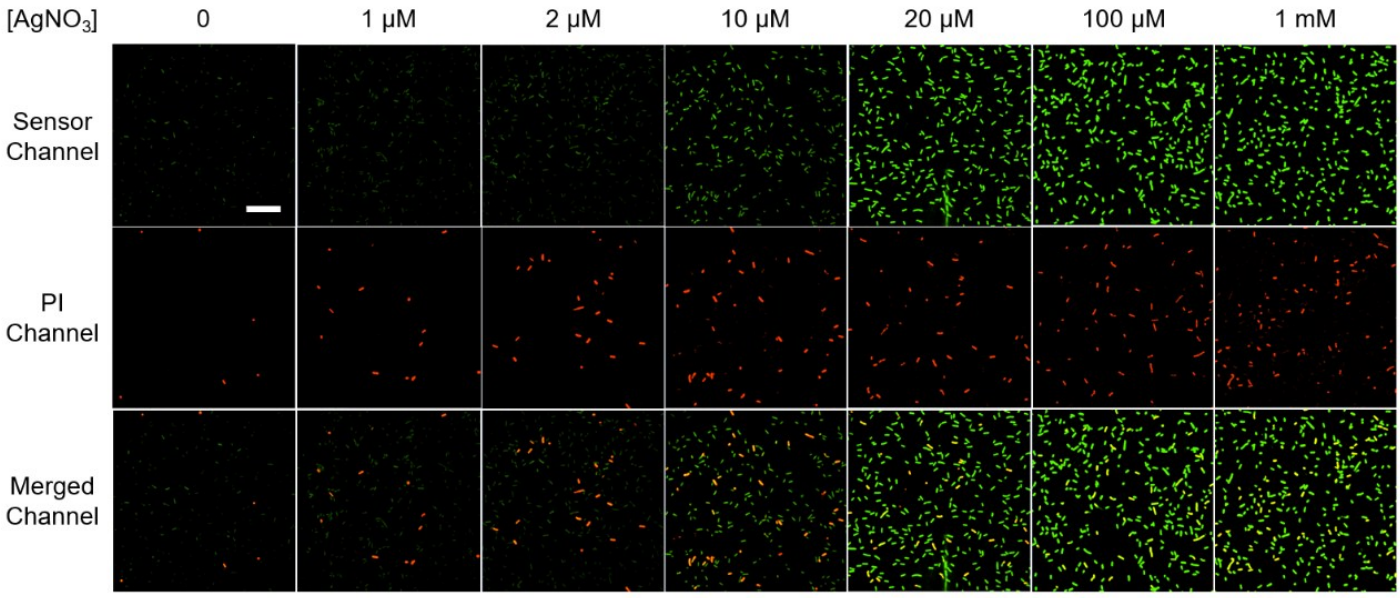


**Figure S6.** Confocal fluorescence imaging of S1-expressing BL21 (DE3)* cells after 2 h incubation with various amounts of $AgNO_3$. The S1 sensor channel (green), propidium iodide channel (red) and merged images are shown. Scale bar: 20 μm. These results indicated that there was an obvious fluorescence intensity increase in the sensor channel after adding 2–100 μM $AgNO_3$. The percentage of PI-stained cells was also increased with the addition of large concentrations of $AgNO_3$.

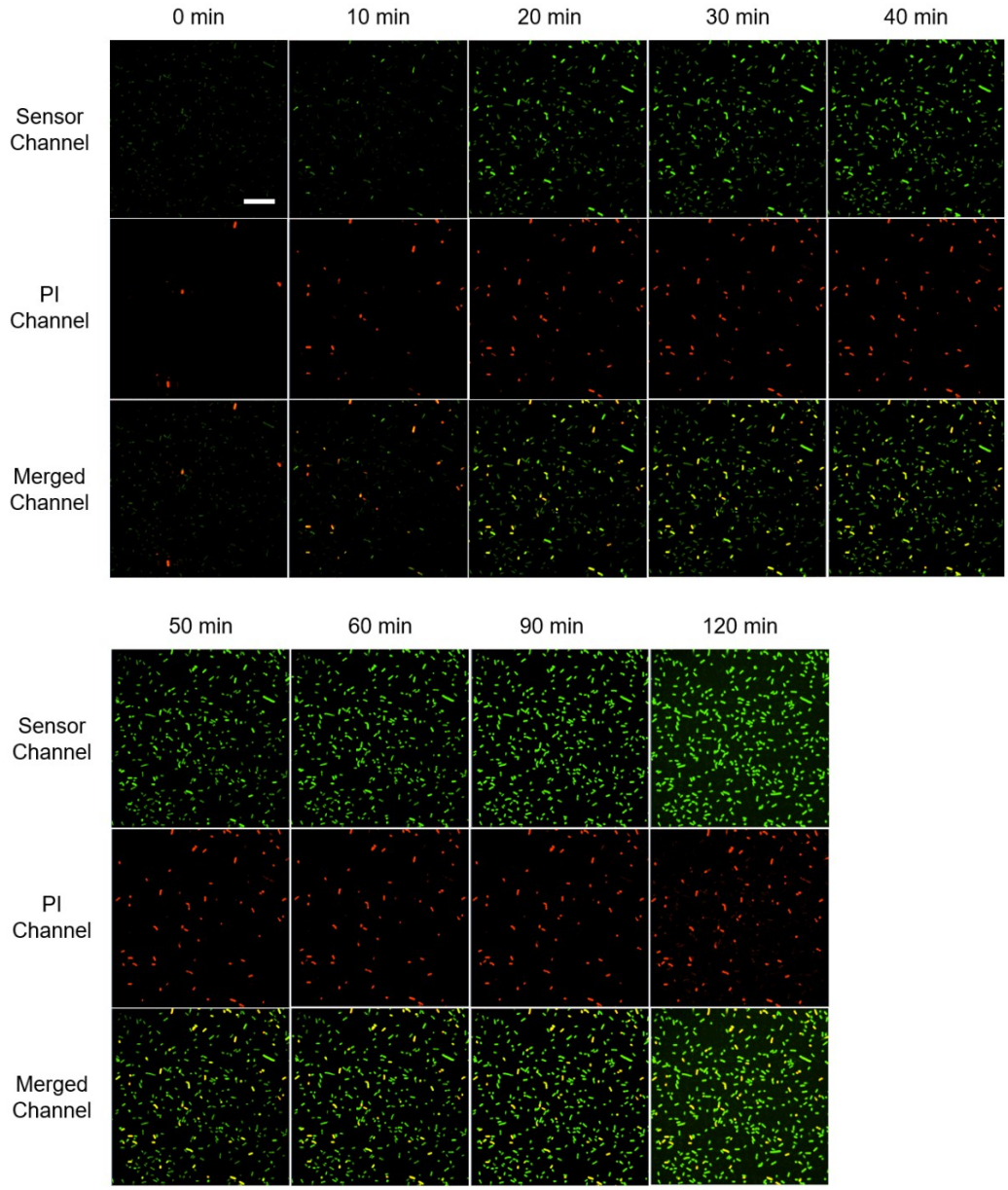


**Figure S7.** Confocal microscopy images of S1-expressing BL21 (DE3)* cells at different time after adding 100 μM $AgNO_3$. Images were taken every 10 min within the first 1 h and then measured at 90 min and 120 min. Fluorescence intensities in both S1 (green) and PI (red) channels were obviously increased during this detection period. There were indeed some cell-to-cell variations in the S1 fluorescence within 1 h period after adding $Ag^+$, while the afterwards signal became more homogeneous. Scale bar: 20 μm.

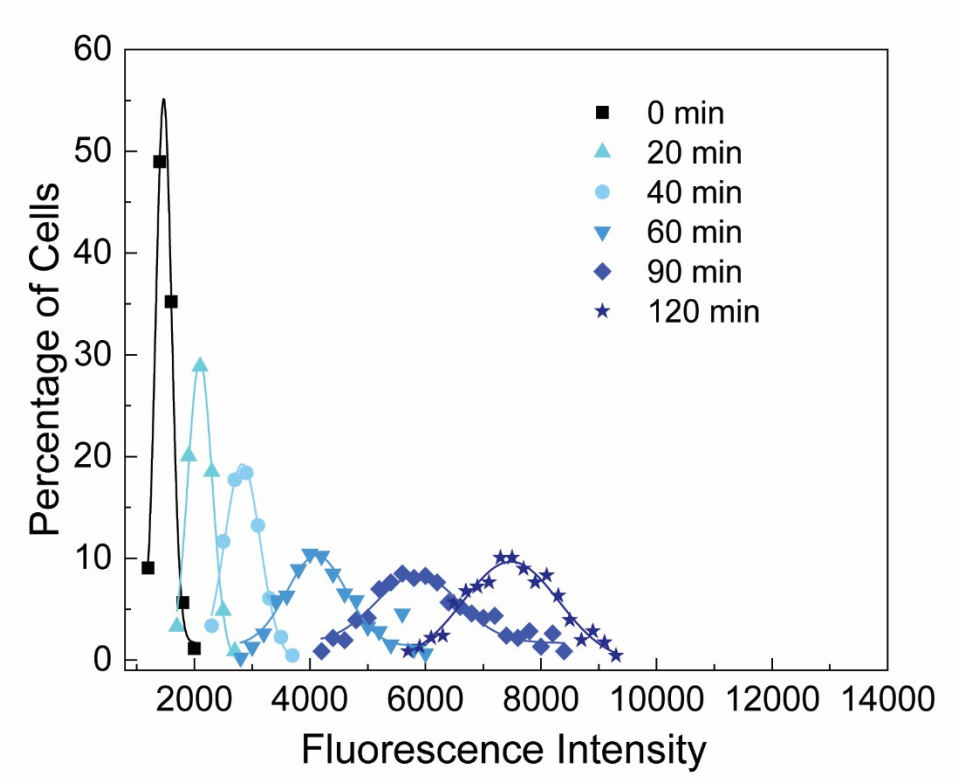


**Figure S8.** Cellular distributions of S1 fluorescence intensities ($Ag^+$ release) at different time point after adding 100 μM $AgNO_3$. Each individual cell was binned according to the brightness (bin size: 200). The percentage of cells in each bin was plotted and fitted with Gaussian distribution curves. A total of 450 cells were measured in each case from three experimental replicates.

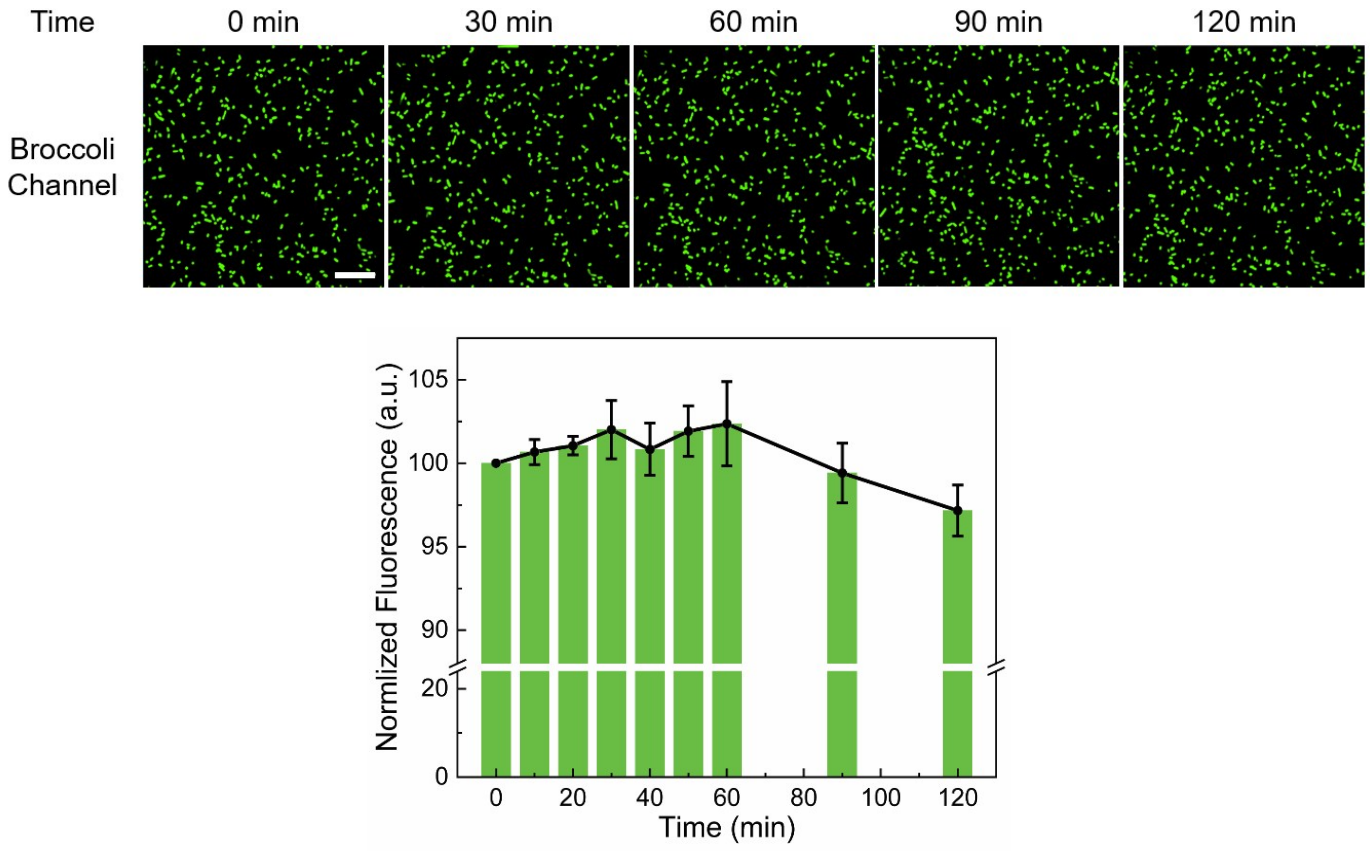


**Figure S9.** Confocal microscopy images in Broccoli-expressing BL21 (DE3)* cells at different time point (top). There was no obvious fluorescence intensity change in Broccoli (green) channel during this 2 h detection period. Scale bar: 20 μm. Bottom is showed the normalized fluorescence signal from confocal microscopy images. Images were taken every 10 min within the first 1 h and then measured at 90 min and 120 min. A total of 1,000 cells were measured in each time point from three experimental replicates and plotted based on the mean and S.E.M. fluorescence intensity. Less than 5% signal changes were observed in 2 h detection period.

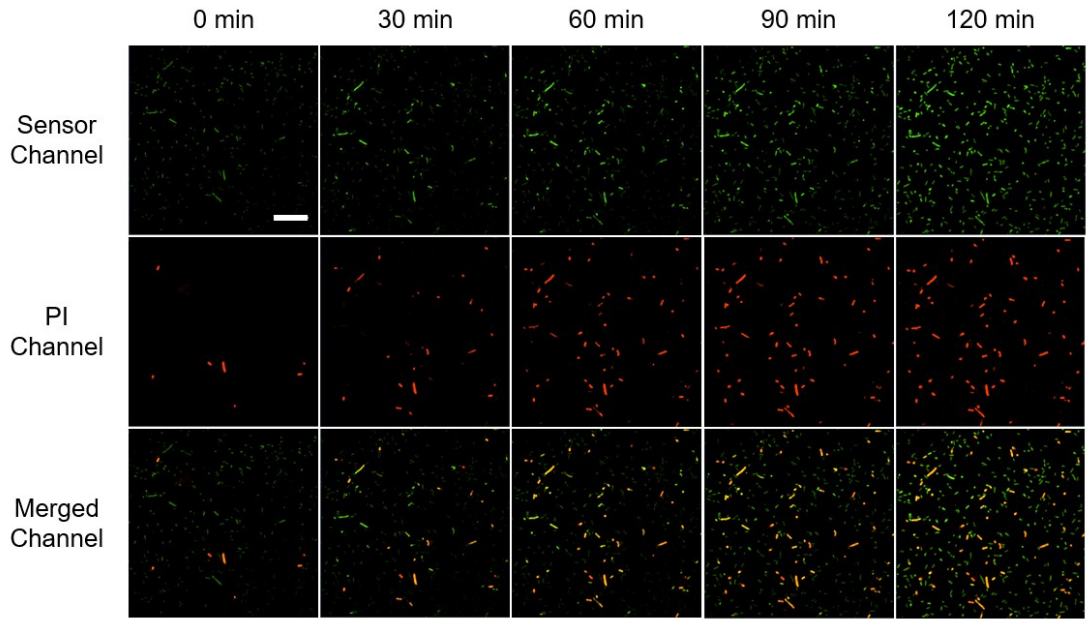


**Figure S10.** Confocal microscopy images in S1-expressing BL21 (DE3)* cells at different time after adding 10 μM $AgNO_3$. Images were taken every 30 min within 2 h. Fluorescence intensities in both S1 (green) and PI (red) channels were obviously increased during this detection period. There were indeed some cell-to-cell variations in the S1 fluorescence within 2 h after adding $Ag^+$. The absolute fluorescence of S1 (green) channel was reduced compared to that of 100 μM $AgNO_3$. Scale bar: 20 μm.

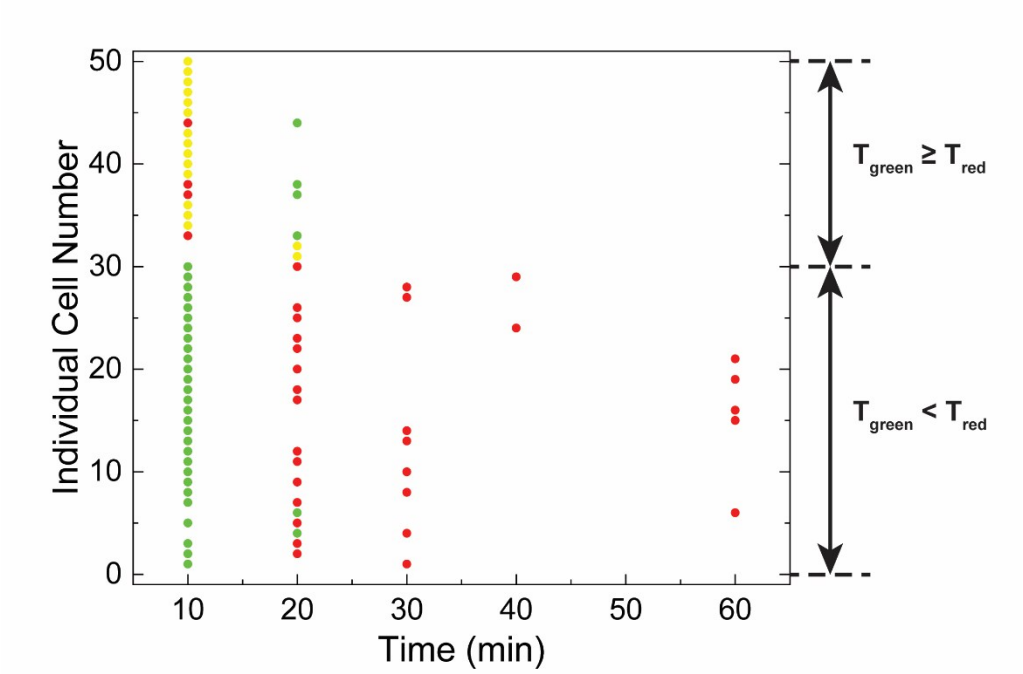


**Figure S11.** Intracellular fluorescence tracking of both green (S1 sensor) and red (PI) channel from 50 individual cells that exhibited high PI signal at 2 h (the same 50 cells as Fig. 3b and 3c). The green and red dots shown the time each cell start to show corresponding fluorescence and the yellow dots shown the overlap of green and red dots. There are in total 30 cells shown green channel at least 10 mins before red channel (30/50 = 60%) and 20 cells shown green channel the same time as or even after red channel (20/50 = 40%).

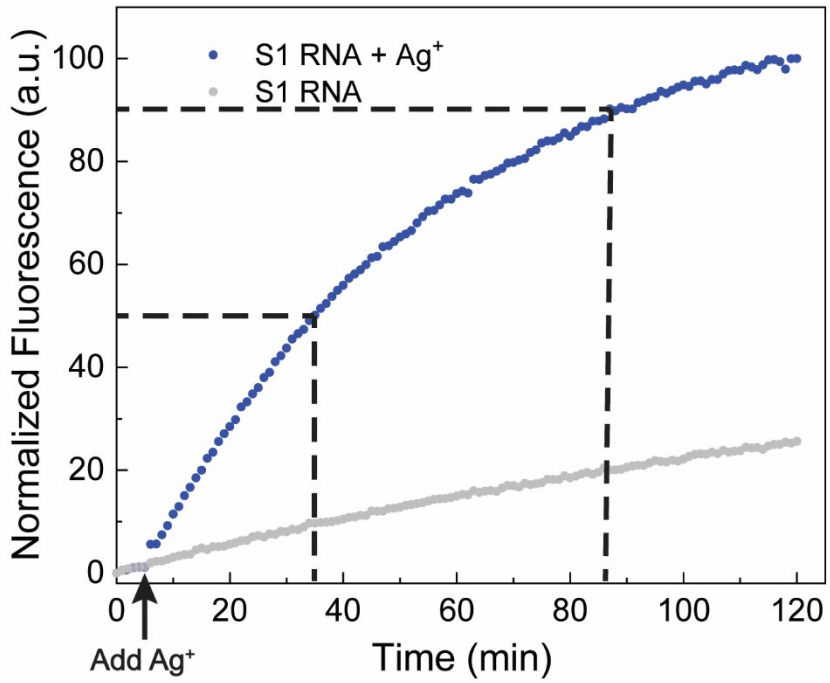


**Figure S12.** Kinetic response of the S1 sensor with (gray dots) and without (blue dots) adding $Ag^+$. The kinetic curve with $Ag^+$ was done by adding 100 μM $AgNO_3$ at 5 min. The fluorescence of S1 without $Ag^+$ was slowly increased. For S1 with $Ag^+$, it took ~30 min to reach half-maximal fluorescence, and ~82 min to reach 90% of maximal signal. Interestingly, these *in vitro* bulk response data were slower compared to the intracellular kinetic response of S1 (maximal within 30 min). It indicated that the cellular $Ag^+$ accumulation rate could be even faster than that shown in these *in vitro* measurements. The difference between cellular and *in vitro* dynamics may be due to the different folding efficiency and local concentration of RNAs within the crowded cellular environment.

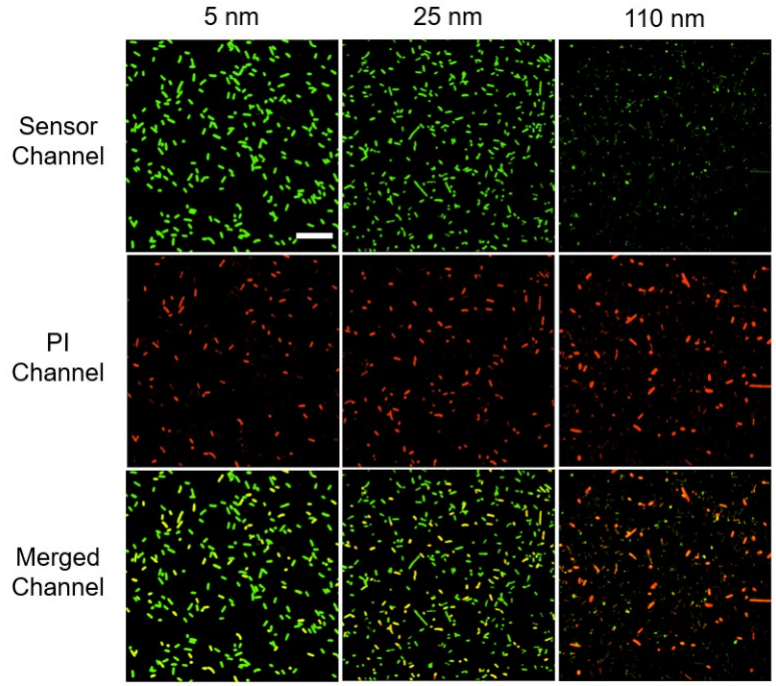


**Figure S13.** Confocal fluorescence imaging of S1-expressing BL21 (DE3)* cells after 2 h incubation with different sizes of PVP-AgNPs. All three sizes (5 nm, 25 nm and 110 nm) of PVP-AgNPs were tested under the same 200 μg/mL concentration. The S1 sensor channel (green), propidium iodide channel (red) and merged images are shown. Scale bar: 20 μm. These results indicated that there was a more obvious fluorescence intensity increase in the sensor channel with smaller size of AgNPs. The percentage of PI-stained cells was also increased as the size of AgNPs reduces.

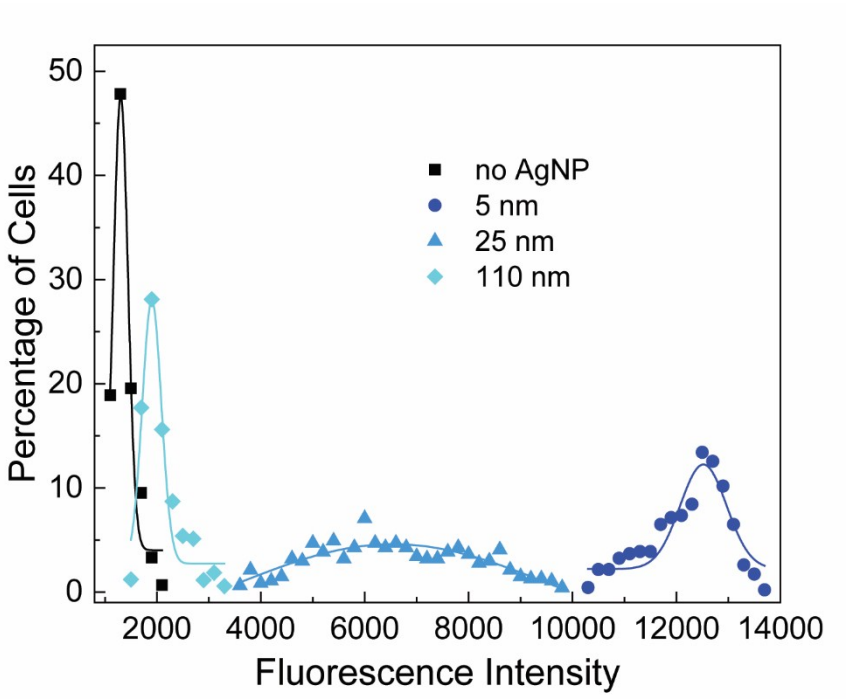


**Figure S14.** Cellular distributions of S1 fluorescence intensities ($Ag^+$ release) from different sizes of AgNPs. Each individual cell was binned according to the brightness (bin size: 200). The percentage of cells in each bin was plotted and fitted with Gaussian distribution curves. A total of 450 cells were measured in each case from three experimental replicates.

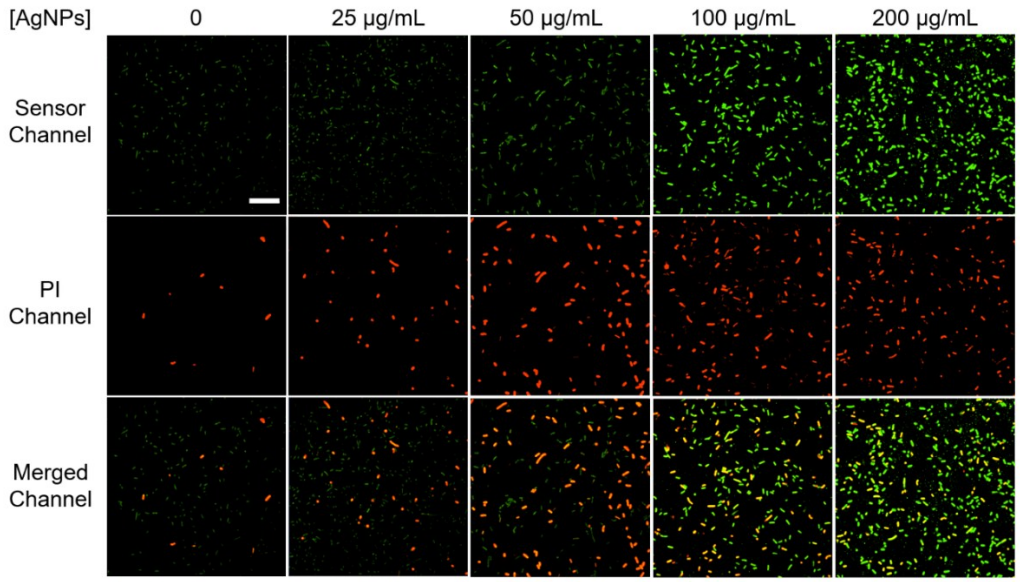


**Figure S15.** Confocal imaging of S1 sensor fluorescence 2 h after adding different concentrations of 25 nm PVP-AgNPs. The S1 sensor channel (green), propidium iodide channel (red) and merged images are shown. Scale bar: 20 μm. These results indicated that there was an obvious fluorescence increase in the sensor channel after adding 50–200 μg/mL 25 nm PVP-AgNPs. The percentage of PI-stained cells was also increased with the addition of 25–100 μg/mL 25 nm PVP-AgNPs, while this percentage was similar between 100 μg/mL and 200 μg/mL concentrations.

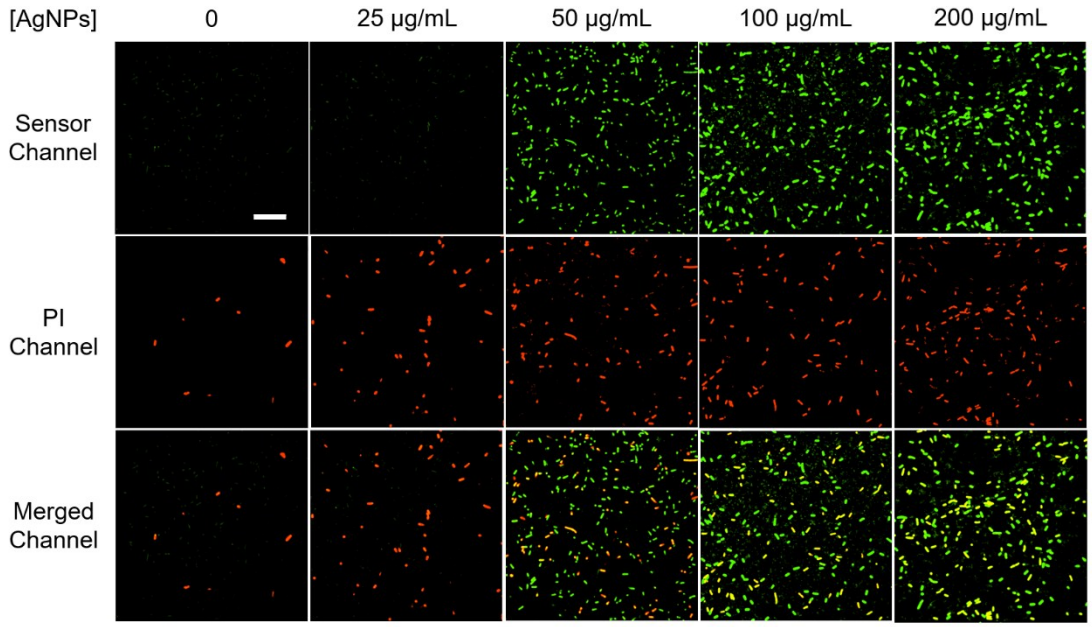


**Figure S16.** Confocal imaging of S1 sensor fluorescence 2 h after adding different concentration of 5 nm PVP-AgNPs. The S1 sensor channel (green), propidium iodide channel (red) and merged images are shown. Scale bar: 20 μm. These results indicated that there was an obvious fluorescence increase in the sensor channel after adding 25–200 μg/mL 5 nm PVP-AgNPs, and these fluorescence intensities were relatively larger compared to 25 nm PVP-AgNPs of the same concentrations. The percentage of PI-stained cells was increased within the concentration range of 25–50 μg/mL, but was at a similar level for 50 μg/mL, 100 μg/mL and 200 μg/mL concentrations.

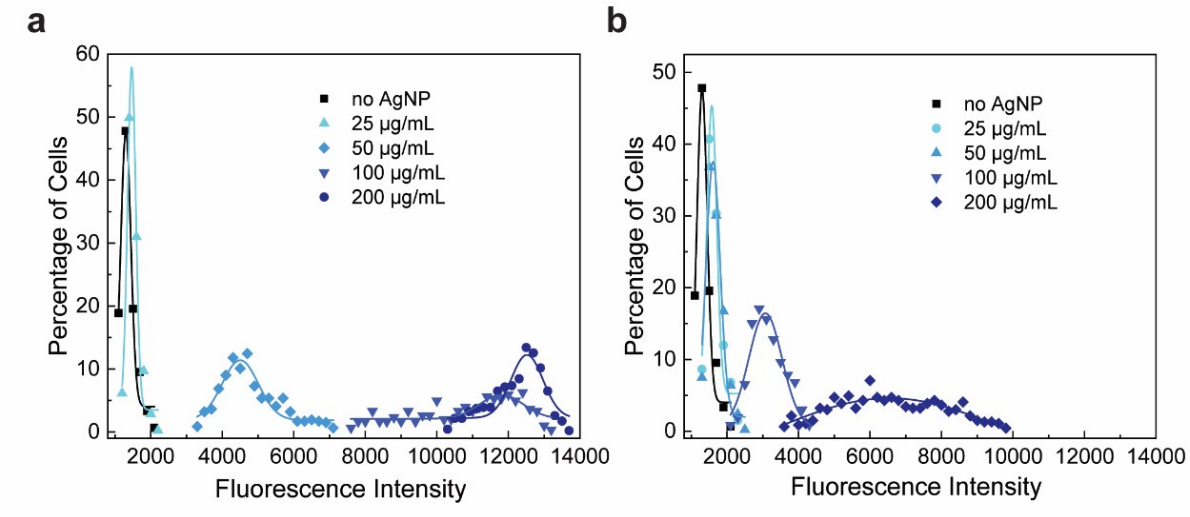


**Figure S17.** Cellular distributions of the S1 fluorescence intensities ($Ag^+$ release) after adding different concentration of (a) 5 nm PVP-AgNPs and (b) 25 nm PVP-AgNPs. Each individual cell was binned according to the brightness (bin size: 200). The percentage of cells in each bin was plotted and fitted with Gaussian distribution curves. A total of 450 cells were measured in each case from three experimental replicates.

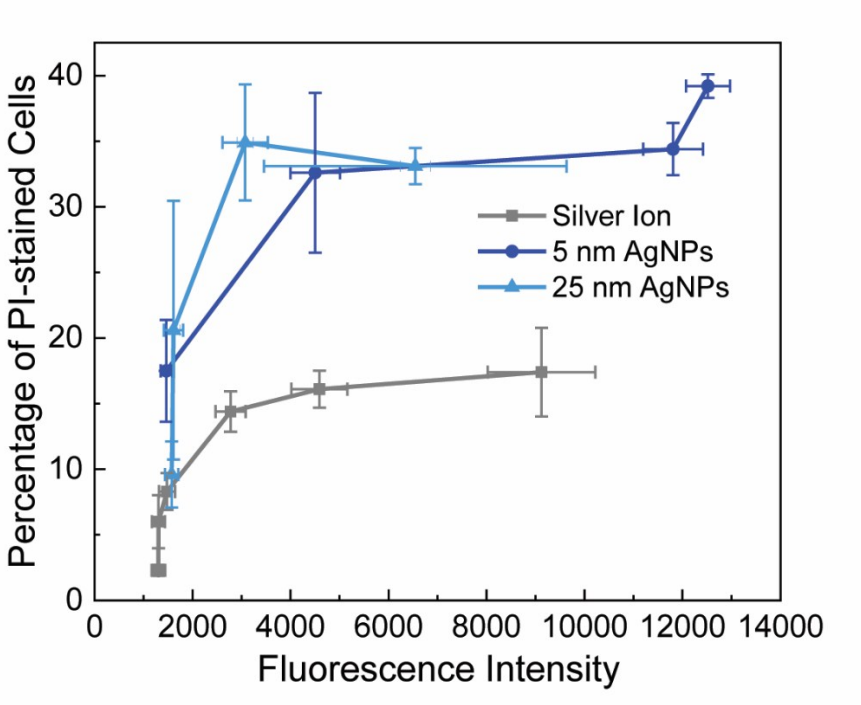


**Figure S18.** The correlation between cellular S1 fluorescence and percentage of PI-stained cells in the cases of $AgNO_3$ (grey), 5 nm AgNPs (light blue), and 25 nm AgNPs (dark blue). Shown are the mean and S.E.M. fluorescence intensities from the Gaussian fitting of S1 channel and calculated mean and S.E.M. percentages from PI channel.